ChemComm

COMMUNICATION

View Article Online
View Journal | View Issue

Cite this: *Chem. Commun.*, 2019, 55, 8615

Received 15th May 2019,
Accepted 23rd June 2019

DOI: 10.1039/c9cc03744f

rsc.li/chemcomm

Water-soluble conjugated polymer with near-infrared absorption for synergistic tumor therapy using photothermal and photodynamic activity†

Sirong Zhou,[a] Changgang Yang,[b] Lixia Guo,[a] Yunxia Wang,*[a] Guofeng Zhang*[b] and Liheng Feng *[a]

A novel near-infrared absorbing photo-agent based on a water-soluble conjugated polymer (PTDBD) is reported for synergetic photothermal/photodynamic therapy with single near-infrared light (808 nm) irradiation. *In vitro* and *in vivo* studies demonstrated the superior therapeutic effect of the single NIR-irradiated PTT/PDT by using PTDBD.

Cancer, as a major cause of death,[1–4] has been the research focus for numerous researchers. Considerable strategies have been developed to treat cancers, such as surgery, chemotherapy, photodynamic therapy (PDT), photothermal therapy (PTT), and immunotherapy.[5–7] Among these therapies, phototherapy based on light and photo-agents shows outstanding advantages including reduced side effects, negligible drug resistance, and spatiotemporal control.[8–11] However, some deficiencies still remain. For PDT, the low penetration depth and oxygen dependence limit further application.[12–15] For PTT, the biosafety, water solubility, photostability and photothermal conversion efficiency (PCE) of the photothermal agents are critical factors influencing the therapeutic effect.[16–18] Therefore, combining two phototherapies together could overcome the shortages of a single therapy.[19–22] Although some efforts have been made to realize a combined therapy, using two different light sources and photo-agents makes the therapy process complicated.[23–26] It is imperative to develop a photo-agent with simultaneous photothermal and photodynamic activity at a single near-infrared (NIR) light irradiation for improved and deeply penetrating cancer therapy.[27–29]

Conjugated polymers (CPs) with outstanding optical and electrical properties have been widely used in chemistry, materials science, and the biological areas.[30–35] Recently, CPs have emerged as potential photo-agents for biomedical applications, especially for PDT and PTT.[36,37] Compared to inorganic materials and small organic molecules, CPs show better biocompatibility, photostability, and degradation in living organisms.[30] Furthermore, their tunable spectra achieved by altering the backbone structures make CPs more appealing to light sources with deep tissue penetration ability, especially for the "therapeutic window" (600–900 nm).[37] There is a great potential to design novel and superior CPs for cancer therapy based on the use of noninvasive light. However, CPs are mostly hydrophobic owing to the large π-conjugated backbone structure. To enhance the water solubility of CPs, amphiphilic polymers are commonly employed to form nanoparticles through mini-emulsions or nanoprecipitation.[38] For a simplified process, water-soluble CPs (WSCPs) were designed by modifying the side chains, which is beneficial for biological application without further encapsulation. Although a series of WSCPs have been reported for bioimaging, gene/drug delivery, antimicrobial and antitumor therapy,[30] NIR-absorbing WSCPs for the phototherapy of tumors with a simultaneous PTT/PDT effect under a single-wavelength and long-wavelength light irradiation are still scarce and warrant further investigation.

In this work, we report a novel water-soluble and NIR-absorbing conjugated polymer (CP) for synergistic antitumor phototherapy (see Scheme 1). By designing the backbone structure *via* a donor–acceptor (D–A) strategy and employing electron-rich thiophene and electron-deficient benzothiadiazole and diketopyrrolopyrrole (DPP), the synthesized CP denoted as PTDBD has an intense absorption in the range of 600–1000 nm, which is just located in the "therapeutic window". Notably, under the irradiation of an 808 nm laser, the PTDBD could efficiently convert light into heat and generate reactive oxygen species (ROS) simultaneously, which circumvent the reduced penetration depth and the inconvenience of multiple light sources. Furthermore, the ROS generated by PTDBD is much greater than that of indocyanine green (ICG) even at a dosage ratio of 1 : 25 (n : n). This could be partly due to the distinct photostability of PTDBD. In addition, the attached cationic quaternary ammonium (QA) groups could enhance the aqueous

[a] *School of Chemistry and Chemical Engineering, Shanxi University, Taiyuan, 030006, P. R. China. E-mail: lhfeng@sxu.edu.cn, wangyunxia@sxu.edu.cn*
[b] *State Key Laboratory of Quantum Optics and Quantum Optics Devices, Institute of Laser Spectroscopy, Shanxi University, Taiyuan, 030006, P. R. China. E-mail: guofeng.zhang@sxu.edu.cn*

† Electronic supplementary information (ESI) available. See DOI: 10.1039/c9cc03744f

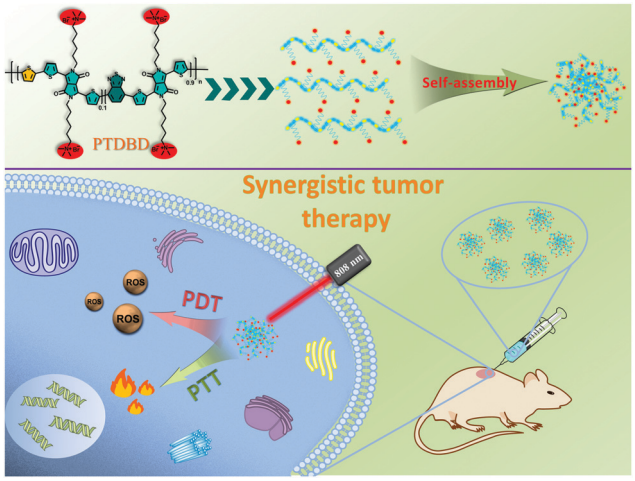

Scheme 1 Schematic illustration of the single NIR-laser-irradiated synergistic PTT/PDT therapy using PTDBD.

solubility of CPs by the self-assembly process. In addition, it also endows PTDBD with the qualities needed to interact with cell membranes. *In vitro* and *in vivo* experiments demonstrated that PTDBD could kill cancer cells and inhibit tumor growth in mice through the synergistic PTT/PDT effect.

Hence, we utilized thiophene as the electron-rich unit and benzothiadiazole and DPP as the electron-deficient units to construct a novel NIR-absorbing CP using the Suzuki coupling reaction (Fig. 1a). Before the polymerization, DPP was modified to synthesize monomer 2 using the respective reaction of 1,6-dibromohexane and *N*-bromosuccinimide according to a previously published report (Fig. S1, ESI†).[39] To improve the aqueous solubility of the hydrophobic DPP-containing polymer, cationic QA groups were introduced onto the side chains. In addition, the facile modification of QA can also facilitate the interaction between polymers and the negatively charged membrane of the tumor cells.

To identify the feasibility of our design, we investigated the photophysical properties of PTDBD. As shown in Fig. 1b, PTDBD has a broad absorption from 600 to 1000 nm in water owing to the strong push–pull electronic effect. Compared to monomers, the absorption of polymer PTDBD was remarkably red-shifted (Fig. S2a, ESI†), which demonstrated that the monomers were conjugated together forming a π-conjugated structure. The emission spectrum of PTDBD was also monitored and no obvious fluorescence emission was observed in the range of 720–900 nm at an excitation wavelength of 700 nm (Fig. S2b, ESI†). The cyclic voltammograms (CV), electron density distributions, and energy band were all investigated (Fig. S3, ESI†), and were found to match the photophysical properties well, demonstrating the low bandgap of the CPs. These results showed that the electron-deficient unit could reduce the lowest unoccupied molecular orbital (LUMO) energy and also the bandgap, which results in the bathochromic shift of the spectrum and facilitates the generation of heat.[37] The hydrophilic side chain and hydrophobic backbone made from the polymer form nanoparticles by self-assembly in water, which can be observed using scanning electron microscopy (SEM) (Fig. 1c). The dynamic light scattering (DLS) measurement also indicated that the hydrodynamic diameter of PTDBD was 280 nm and the solution was clear and stable (Fig. 1d).

Considering the fact that PTDBD has a strong absorption in the NIR range and no obvious fluorescence emission, we further investigated the photothermal performance of PTDBD. As shown in Fig. 2a, obvious temperature changes to the PTDBD solution with various concentrations were observed upon irradiation with an 808 nm laser at a power density of 1 W cm^{-2} for 8 min. At a low concentration of 60 μg mL^{-1}, the temperature of the solution increased to 65 °C, which demonstrated the good photothermal conversion capability of PTDBD. Thermal images were also collected to visualize the temperature changes of the PTDBD solution with different concentrations and prolonged time (Fig. 2b). Furthermore, we investigated the photothermal response of the PTDBD solution to different laser

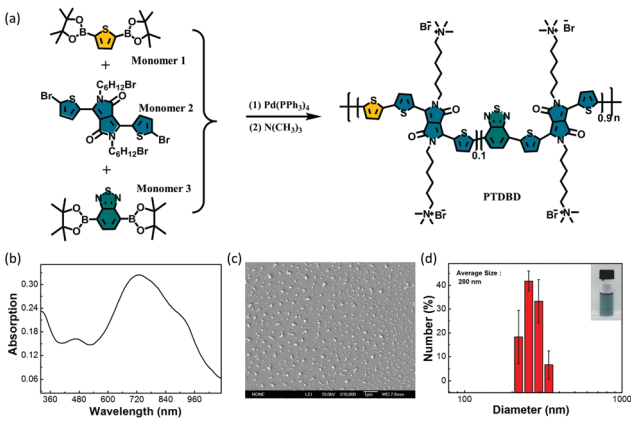

Fig. 1 (a) Synthetic route for the water-soluble PTDBD. (b) UV-vis-NIR absorption spectrum of PTDBD in water (20 μg mL^{-1}). (c) SEM image of PTDBD. (d) Hydrodynamic size distribution of PTDBD in water measured using DLS. The inset shows a photograph of the PTDBD aqueous solution (50 μg mL^{-1}).

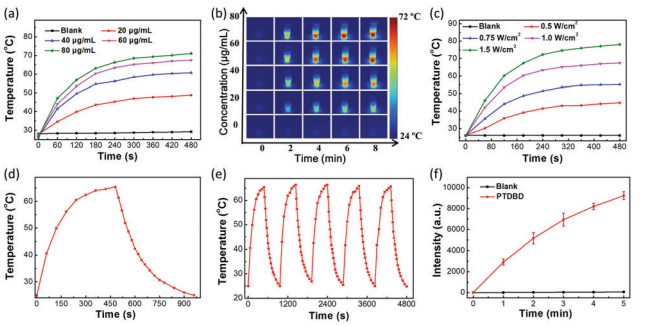

Fig. 2 (a) Temperature elevation and (b) thermal images of the PTDBD aqueous solution with various concentrations under laser irradiation (808 nm, 1 W cm^{-2}). (c) Temperature elevation of the PTDBD aqueous solution (60 μg mL^{-1}) under irradiation at different power densities of an 808 nm laser. (d) Photothermal response of the PTDBD aqueous solution (60 μg mL^{-1}) under laser irradiation (808 nm, 1 W cm^{-2}) for 8 min and then the laser was shut off. (e) Temperature profiles of the PTDBD aqueous solution (60 μg mL^{-1}) for five cycles of ON/OFF laser irradiation. (f) ROS generation of PTDBD aqueous solution (4 μg mL^{-1}) under the irradiation of an 808 nm laser (1 W cm^{-2}).

densities, which demonstrated that the photothermal profile was power density-dependent (Fig. 2c). Next, we investigated the PCE of PTDBD according to the previously reported method,[37] and the PCE was calculated to be 31% (Fig. 2d and Fig. S4, ESI†). This was higher than those reported for the inorganic photothermal materials, such as Au nanorods and CuS nanocrystals.[37] Furthermore, the photothermal stability of PTDBD was evaluated as shown in Fig. 2e, PTDBD gave almost the same photothermal effect after irradiation using a 808 nm laser for 8 min and the same irradiation was repeated four times after cooling the solution back to the original temperature. The result showed the excellent photothermal capability of PTDBD and the potential for it to be used as a photothermal material for PTT. It has been reported that DPP-based molecules can generate ROS,[24] therefore we used a classic assay based on 2,7-dichlorofluorescein diacetate (DCFH-DA) to evaluated the ROS generating ability of PTDBD under the irradiation of an 808 nm laser. As shown in Fig. 2f, the fluorescence intensity of DCF in the presence of PTDBD increased with prolonged time, indicating the generation of ROS. Compared with ICG, a typical NIR sensitizer, PTDBD could generate more ROS, even after increasing the dosage of ICG to 25-fold (Fig. S5a, ESI†). It was also found to be better than our previously reported polymer,[40] and generated significantly more ROS in white light (Fig. S5b and c, ESI†). These results illustrate that PTDBD has good ROS generation capability under the irradiation of light from the long wavelength NIR region, which could circumvent the reduced penetration depth of common photosensitizers for PDT. The dual photoconversion ability of PTDBD under the irradiation of a NIR laser make it a promising photo-active agent for the killing of cancer cells with a synergetic PTT and PDT effect.

After verification of the photo-active properties of PTDBD, we used a standard methyl thiazolyl tetrazolium (MTT) assay to evaluate the synergetic killing ability against HeLa cells (Fig. 3a). The cells treated with PTDBD were mostly alive ($>80\%$) without light irradiation, even at concentrations of up to 100 μg mL^{-1}. However, those cells exposed to NIR light (1 W cm^{-2}) for 8 min were killed with different degrees of success using different therapies. When the PTDBD concentration increased, the therapeutic effect of PDT showed no remarkable change, while the effect of PTT increased obviously. At an incubation concentration of 100 μg mL^{-1} the cells were almost killed using the synergetic PDT/PTT effect. To further visualize the cell viability, confocal laser scanning microscopy (CLSM) was performed (Fig. 3b). Only cells treated with PTDBD and irradiated using the NIR laser were stained with ethidium bromide (EB) and emitted red fluorescence, which indicated the cells were dead. In contrast, treatment with PTDBD and NIR laser irradiation did not damage the cell viability, and cells were stained with acridine orange (AO), a live cell dye, and emitted a green fluorescence. By changing the power density of the laser and the irradiation time, the cell viability was affected (Fig. S6, ESI†). The temperature changes of the HeLa cells treated with PTDBD (100 μg mL^{-1}) were monitored, as shown in Fig. 3c, and the photothermal images are also shown. The living cells could not survive at the high temperature of 60 °C. The intracellular ROS generation by

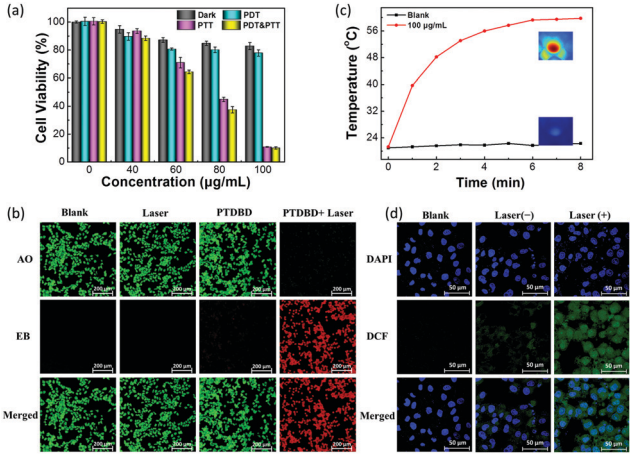

Fig. 3 (a) Cell viability of HeLa cells using different therapies under irradiation from a 808 nm laser (1 W cm^{-2}, 8 min) after treatment with various concentrations of PTDBD. (b) CLSM images of HeLa cells stained with AO (live cells, green fluorescence) and EB (dead cells, red fluorescence) after various treatments. (c) Photothermal curves of HeLa cells with and without treatment with PTDBD (100 μg mL^{-1}) under the irradiation of an 808 nm laser (1 W cm^{-2}, 8 min). The inset images show the corresponding thermal images. (d) Fluorescence images of the HeLa cells incubated with DCFH-DA, DAPI and PTDBD after different treatments.

PTDBD under NIR irradiation was verified using a DCFH-DA assay. As shown in Fig. 3d, the green florescence of DCF was observed in the cells irradiated by the laser, indicating ROS generation inside the cell. All of these results showed that PTDBD could kill cancer cells by the synergetic phototherapy of PTT and PDT.

To investigate the potential of PTDBD for practical antitumor applications, we established a HeLa tumor-bearing nude mouse model. All mice were divided into four groups, these were: saline, saline + laser, PTDBD, and PTDBD + laser. After intratumoral injection, the laser and PTDBD + laser groups were irradiated with an 808 nm laser at a power density of 1 W cm^{-2} for 10 min. The infrared thermal images and temperature changes were recorded and are shown in Fig. 4a and b. In the presence of PTDBD, the temperature of the tumor rapidly increased to 51 °C upon irradiation, while the saline in the tumor could not generate heat resulting in a tumor temperature of 41 °C. After 21 days of treatment, the tumors of the mice in the phototherapy group were effectively ablated (Fig. 4c and Fig. S7, ESI†). Laser and PTDBD alone could not inhibit the growth of the tumor as evidenced by measuring of the tumor sizes (Fig. 4d). All of the mice in the four groups showed no change in their body weight (Fig. 4d), indicating the biosafety of laser irradiation, PTDBD, and phototherapy. Furthermore, the major organs of the mice were extracted and stained using hematoxylin and eosin (H&E). As shown in Fig. S8 (ESI†), no noticeable damage was observed in all groups, indicating that PTDBD is safe for antitumor therapy.

In summary, we synthesized a novel water-soluble and NIR-absorbing conjugated polymer PTDBD for the synergetic phototherapy of cancers. By conjugating the "D–A" and "A–A" structural units, PTDBD has a broad and strong NIR absorption, ranging

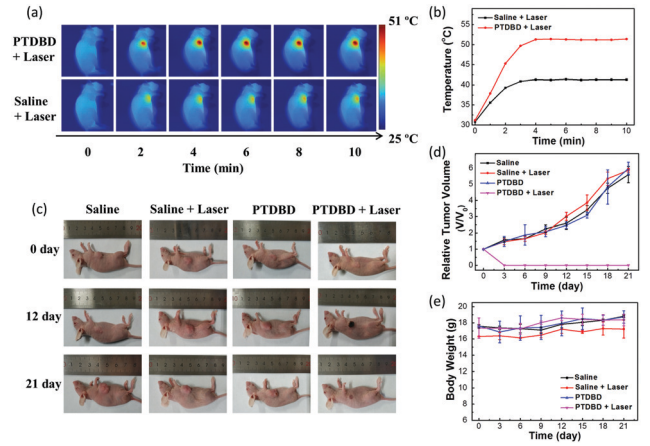

Fig. 4 (a) Thermal images of HeLa tumor-bearing mice under the irradiation of an 808 nm laser (1 W cm^{-2}) after injection of saline and PTDBD, respectively. (b) Photothermal profiles of tumors in mice under the irradiation of an 808 nm laser (1 W cm^{-2}). (c) Representative photographs of HeLa tumor-bearing mice after different treatments for different time periods. (d) Tumor volume and (e) body weight changes of mice during different treatments.

from 600–1000 nm. Cationic QA group modified side chains allow the CPs to easily assemble to form nanoparticles in water and facilitate the interaction with the membrane. These photostable nanoparticles could effectively convert NIR light (808 nm) into heat and ROS simultaneously at both the molecular and cellular level. *In vitro* and *in vivo* experiments demonstrate that PTDBD can effectively kill HeLa cells and eliminate tumors in mice using synergetic PTT/PDT treatment with good biosafety. This research provides a theoretical foundation for the design of NIR-responsive agents with superior dual photothermal and photodynamic activity, and offers promising photo-agents for simplified clinical tumor therapy.

This work is supported by the National Nature Science Foundation (No. 21807067, 21571116 and 21601111), the Program for the Outstanding Innovative Teams of Higher Learning Institutions of Shanxi (No. 2017-07), and the SanJin Scholars Support Plan under Special Funding (No. 2017-06).

Conflicts of interest

There are no conflicts to declare.

Notes and references

1 L. Torre, F. Bray, R. Siegel, J. Ferlay, J. Lortet-Tieulent and A. Jemal, *Ca-Cancer J. Clin.*, 2015, **65**, 87–108.
2 W. Zhao, J. Hu and W. Gao, *ACS Appl. Mater. Interfaces*, 2017, **9**, 23528–23535.
3 B. Li, Q. Sun, Z. Yu, X. Gao, W. Pan, X. Wan and B. Tang, *ACS Nano*, 2018, **12**, 5197–5206.
4 W. Zhao, Y. Yang, L. Song, T. Kang, T. Du, Y. Wu, M. Xiong, L. Luo, J. Long, K. Men, L. Zhang, X. Chen, M. Huang and M. Gou, *Adv. Sci.*, 2018, **5**, 1700263.
5 W. Deng, Q. Wu, P. Sun, P. Yuan, X. Lu, Q. Fan and W. Huang, *Polym. Chem.*, 2018, **9**, 2805–2812.
6 H. Yoon, S. Selvan, Y. Yang, M. Kim, D. Yi, I. Kwon and K. Kim, *Biomaterials*, 2018, **178**, 597–607.
7 C. Ng, J. Li and K. Pu, *Adv. Funct. Mater.*, 2018, **28**, 1804688.
8 L. Cheng, C. Wang, L. Feng, K. Yang and Z. Liu, *Chem. Rev.*, 2014, **114**, 10869–10939.
9 Y. Zhou, X. Liang and Z. Dai, *Nanoscale*, 2016, **8**, 12394–12405.
10 R. Xing, K. Liu, T. Jiao, N. Zhang, K. Ma, R. Zhang, Q. Zou, G. Ma and X. Yan, *Adv. Mater.*, 2016, **28**, 3669–3676.
11 J. Zhang, C. Yang, R. Zhang, R. Chen, Z. Zhang, W. Zhang, S. Peng, X. Chen, G. Liu, C. S. Hsu and C. S. Lee, *Adv. Funct. Mater.*, 2017, **27**, 1605094.
12 Y. Shi, S. Liu, Y. Liu, C. Sun, M. Chang, X. Zhao, C. Hu and M. Pang, *ACS Appl. Mater. Interfaces*, 2019, **11**, 12321–12326.
13 Y. Yuan, J. Liu and B. Liu, *Angew. Chem., Int. Ed.*, 2014, **53**, 7163–7168.
14 W. Wu, G. Feng, S. Xu and B. Liu, *Macromolecules*, 2016, **49**, 5017–5025.
15 M. Li, T. Xiong, J. Du, R. Tian, M. Xiao, L. Guo, S. Long, J. Fan, W. Sun, K. Shao, X. Song, J. W. Foley and X. Peng, *J. Am. Chem. Soc.*, 2019, **141**, 2695–2702.
16 Y. Zhang, C. Y. Ang, M. Li, S. Y. Tan, Q. Qu and Y. Zhao, *ACS Appl. Mater. Interfaces*, 2016, **8**, 6869–6879.
17 J. T. Robinson, S. M. Tabakman, Y. Liang and H. Wang, *J. Am. Chem. Soc.*, 2011, **133**, 6825–6831.
18 S. Luo, Z. Yang, X. Tan, Y. Wang, Y. Zeng, Y. Wang, C. Li, R. Li and C. Shi, *ACS Appl. Mater. Interfaces*, 2016, **8**, 17176–17186.
19 B. Jiang, L. Hu, X. Shen, S. Ji, Z. Shi, C. Liu, L. Zhang and H. Liang, *ACS Appl. Mater. Interfaces*, 2014, **6**, 18008–18017.
20 Z. Zhang, J. Wang and C. Chen, *Adv. Mater.*, 2013, **25**, 3869–3880.
21 E.-K. Lim, T. Kim, S. Paik, S. Haam, Y.-M. Huh and K. Lee, *Chem. Rev.*, 2015, **115**, 327–394.
22 X.-L. Guo, Z.-Y. Ding, S.-M. Deng, C.-C. Wen, X.-C. Shen, B.-P. Jiang and H. Liang, *Carbon*, 2018, **134**, 519–530.
23 H. Xiang, F. Xue, T. Yi, H. Tham, J. Liu and Y. Zhao, *ACS Appl. Mater. Interfaces*, 2018, **10**, 16344–16351.
24 Y. Cai, P. Liang, Q. Tang, X. Yang, W. Si, W. Huang, Q. Zhang and X. Dong, *ACS Nano*, 2017, **11**, 1054–1063.
25 S. Goel, C. A. Ferreira, F. Chen, P. A. Ellison, C. M. Siamof, T. E. Barnhart and W. Cai, *Adv. Mater.*, 2018, **30**, 1704367.
26 J. Ge, Q. Jia, W. Liu, M. Lan, B. Zhou, L. Guo, H. Zhou, H. Zhang, Y. Wang, Y. Gu, X. Meng and P. Wang, *Adv. Healthcare Mater.*, 2016, **5**, 665–675.
27 Z. Sheng, D. Hu, M. Zheng, P. Zhao, H. Liu, D. Gao, P. Gong, G. Gao, P. Zhang, Y. Ma and L. Cai, *ACS Nano*, 2014, **8**, 12310–12322.
28 A. Kumar, S. Kumar, W.-K. Rhim, G.-H. Kim and J.-M. Nam, *J. Am. Chem. Soc.*, 2014, **136**, 16317–16325.
29 J. Lin, S. Wang, P. Huang, Z. Wang, S. Chen, G. Niu, W. Li, J. He, D. Cui, G. Lu, X. Chen and Z. Nie, *ACS Nano*, 2013, **7**, 5320–5329.
30 C. Zhu, L. Liu, Q. Yang, F. Lv and S. Wang, *Chem. Rev.*, 2012, **112**, 4687–4735.
31 H. Peng and D. T. Chiu, *Chem. Soc. Rev.*, 2015, **44**, 4699–4722.
32 K. Pu, N. Chattopadhyay and J. Rao, *J. Controlled Release*, 2016, **240**, 312–322.
33 J. Li and K. Pu, *Chem. Soc. Rev.*, 2019, **48**, 38–71.
34 Y. Wang, L. Feng and S. Wang, *Adv. Funct. Mater.*, 2018, **29**, 1806818.
35 X. Lu, P. Yuan, W. Zhang, Q. Wu, X. Wang, M. Zhao, P. Sun, W. Huang and Q. Fan, *Polym. Chem.*, 2018, **9**, 3118–3126.
36 Z. Meng, W. Hou, H. Zhou, L. Zhou, H. Chen and C. Wu, *Macromol. Rapid Commun.*, 2018, **39**, 1700614.
37 S. Li, X. Wang, R. Hu, H. Chen, M. Li, J. Wang, Y. Wang, L. Liu, F. Lv, X. Liang and S. Wang, *Chem. Mater.*, 2016, **28**, 8669–8675.
38 S. Li, T. Chen, Y. Wang, L. Liu, F. Lv, Z. Li, Y. Huang, K. S. Schanze and S. Wang, *Angew. Chem., Int. Ed.*, 2017, **56**, 13455–13458.
39 Y. Cai, Q. Tang, X. Wu, W. Si, Q. Zhang, W. Huang and X. Dong, *ACS Appl. Mater. Interfaces*, 2016, **8**, 10737–10742.
40 Y. Wang, H. Wang, L. Guo, Y. Pang and L. Feng, *ACS Appl. Mater. Interfaces*, 2018, **10**, 34878–34885.

